ISSN (Print) : 0974-6846
ISSN (Online) : 0974-5645
Indian Journal of Science and Technology, *Vol 10(34), DOI: 10.17485/ijst/2017/v10i34/116671, September 2017*

Nano Particle (Metallic Copper and Cadmium sulphide) Application: Photocatalytic Potentiality and Antimicrobial Effectivity

Divya Vishambhar Kumbhakar[1], Animesh Kumar Datta[1]*, Debadrito Das[1], Venu Prabha Sahu[2], Sukhdeo B. Barbuddhe[2], Suraj Sharma[2], Bapi Ghosh[1] and Ankita Pramanik[1]

[1]Department of Botany, Cytogenetics, Genetics and Plant breeding Section, Kalyani University, Kalyani, Nadia - 741235, West Bengal, India;
kumbhakardivya@gmail.com, dattaanimesh@gmail.com, debadritodassmailbox@gmail.com, bpghosh88@gmail.com, ankitapramanik15@gmail.com
[2]Indian Council of Agricultural Research-National Institute of Biotic Stress Management, Baronda, Raipur - 493225, Chattisgarh, India;
sahuvenu2@gmail.com, barbuddhesb@gmail.com, suraj.sharma869@gmail.com

Abstract

Objectives: Use of nanoparticles (Cu- and CdS-NPs) in mineralization of azo dyes (methyl red and malachite green) for waste water management and effectivity against serotypes of *Listeria monocytogenes* and *Salmonella typhimurium*. **Methods**: To study azo-dyes mineralization potentiality, dye-NPs reaction mixtures are analyzed using UV-vis near infra-red spectroscopy, HPLC and UPLC-ESI-QTOF-MS. Antimicrobial effectivity of NPs is studied following quantification of inhibition zone from disc diffusion assay. NPs mediated bacterial cell cycle inhibition is analyzed following flow cytometry. **Findings**: The proposed MG degradation pathways using Cu- and CdS- NPs are pioneering reports. Dye mineralization efficiency of Cu-NPs is found to be higher than CdS-NPs. On the basis of analysis of reaction intermediates (using HPLC, ESI-QTOF-MS), separate dye degradation pathways are proposed. Disc diffusion assay reveals antimicrobial effectivity of NPs for controlling human pathogenic bacteria. Flow cytometry can be used as efficient tool for ascertaining NPs mediated microbial growth inhibition. **Application**: Photocatalytic potentiality of the prepared NPs can be effectively used for removal of azo-dyes contaminants from waste water. NPs can also be effectively used against studied human pathogenic bacteria for drug designing.

Keywords: Azo-dyes; Antimicrobial Potentiality, Cu- and CdS-NPs, FACs, Photocatalysis

1. Introduction

Nanoparticles (at least one dimension <100 nm[1]) possessing specific physico-chemical properties as strength, high surface to volume ratio, wide excitation binding energy[2], specialized conductivity[3] among others, confers strong chemo-reactive ability as well as high oxidation

*Author for correspondence

potentiality for degradation of organic compounds[4,5]. Azo-dyes (methyl red-MR and malachite green-MG) are organic compounds widely released as industrial effluents causing aquatic toxicity[6] and health problems[7]. Chemo-reactive and catalytic potentialities of nano dimensional class compounds are used for photocatalytic degradation of azo-dyes[8] which is significant for waste water management[9,10].

Apart from the nano-mediated photocatalytic activity, nanomaterials have got another important application in the control of human pathogenic bacteria[11,12]. Further, applications for nano materials can be effectively explored for drug designing and its targeted delivery in the affected physiological system.

Present study highlights the application module undermined, and encompasses assessment of photocatalytic efficiency (using UV-visible near infra-red spectroscope) of the synthesized and opto-physically characterized[13] copper (Cu) and cadmium sulphide (CdS) nanoparticles (NPs). Furthermore, based on the identification (using High Performance Liquid Chromatography, HPLC) and quantification (Ultrapure Liquid Chromatography-Electron Spray Ionization-Quantitative time of flight Mass Spectroscopy, UPLC-ESI-QTOF-MS) of intermediate by-products, the possible reaction pathways are proposed for complete mineralization of both the dye compounds. Moreover, antimicrobial activity of the prepared nano-suspensions is assessed using human pathogenic bacteria namely, *Listeria monocytogenes* (gram positive bacillus, ILCC 293 of serotype 1/2b and ILCC 041a of serotype 1/2a) and *Salmonella typhimurium* (gram negative bacillus, collected from diseased person and subsequently cultured and characterized). Flow cytometry is performed for determination of bacterial growth kinetics under NPs stressed conditions.

2. Methodology

2.1 Synthesis and Characterization of nanomaterials

Wet chemical synthesis of nanomaterials was done as proposed by Chatterjee et al.[14] for Cu-NPs (metallic) and Halder et al.[15] for CdS-NPs (semiconductor also known as QDs). The prepared nanoparticles were characterized opto-physically[13] for nanostandard quality assurance.

2.2 Assessment of photocatalytic potentiality

Photocatalytic reaction system was prepared using two model dyes namely, methyl red (MR) and malachite green (MG) (3×10^{-5} M dilution in milli-Q water) and nanosuspensions (10 µg/ml) in 9:1 ratio. Resultant mixtures were stirred for 20 min in absolute dark condition (temperature: 25±1°C; pH: 8.0 for Cu-NPs, 9.3 for CdS-NPs) and subsequently irradiated under Xenon lamp (source to distance 10 cm, 50 mW, irradiation wavelength: λ>420 nm) as artificial source of light for 2h. Reaction mixtures were analyzed using UV-visible near infra-red spectrometer (Shimadzu UV-1800; range: 190-1200 nm) at an interval of 30 minutes and the respective optical density values were recorded. Concentrations of photolytically degrading dyes were quantified by HPLC (Chromaster, Hitachi with UV-vis detector, flow rate – 0.4 ml/min, solvent – methanol:water :: 85:15, detection wavelength: 425 nm for MR and 618 nm for MG; RP C-18 column – 4.6 mm×250mm with 5.0 µm particle size). Reaction intermediates were separated and identified using UPLC-ESI-QTOF-MS (Xevo G2-XS QTOF, Waters, C-18 analytical column of 2.00 mm × 150 mm with 3.0 µm particle size, flow rate: 0.2 ml/min, voltage – 3.8 kV, nebulizer pressure 50 psi).

2.3 Assessment of antimicrobial activity

2.3.1 Bacterial strains and serotypes

Different isolates of *Listeria monocytogenes*– *L. monocytogenes* MTCC 1143 serotype 4b (ILCC 293 of serotype 1/2b isolated from milk and ILCC 041a of serotype 1/2a isolated from cattle) were procured from Indian Listeria Culture Collection (ILCC), ICAR-National Institute of Biotic Stress Management, Raipur, Chhattisgarh and were maintained in brain-heart infusion (BHI: Difco™, Dickson and Company, Sparks, MD, USA) broth in 15% glycerol.

Salmonella typhimurium strain was obtained from ICAR-National Institute of Biotic Stress Management, Raipur, and Chhattisgarh and was maintained in nutrient broth.

2.3.2 Preparation of NPs dilutions

Stock nanosuspensions of both Cu- and CdS-NPs (10 mg/ml) were diluted (10, 15 and 20 µg/ ml) in sterilized mili-Q water for disc diffusion assay.

2.3.3 Disc diffusion assay

Both isolates of *L. monocytogenes* (2 ml) were inoculated in BHI broth and incubated in shaking condition (150 rpm) for overnight at 37˚C. Optical densities (OD) of both the bacterial suspensions were measured at 600 nm. The broth suspensions of the strains (0.1 ml each) were plated uniformly on the surface of BHI agar plates employing sterile cottons swabs– HiMEDIA. *S. typhimurium* was inoculated in 2 ml nutrient broth and incubated for 24 h at 37˚C. OD was measured at 600 nm and the bacterial cells (0.1 ml) were plated on nutrient agar with sterile cotton swabs and incubated at 37˚C. The paper discs (HiMEDIA) of about 6 mm diameter were sterilized and soaked in the prepared nano-dilutions. NPs laden discs were then separately placed on culture plates and subsequently incubated at 37˚C for 24 h. Diameter of inhibition zone was measured to nearest millimetre. Ampicillin disc (HiMEDIA) was used as control. The disc diffusion assay was performed in triplicates for consistent outcome.

2.3.4 FACs analysis of bacterial suspension

Suspensions of both *L. monocytogenes* and *S. typhimurium* were treated with 10 µg/ml of Cu- and CdS-NPs for 3 hours at 37°C. The treated cells (50µl) were washed in 1M (pH 8.0) phosphate buffer saline (PBS buffer, SRL, India) and was co-incubated in propidium iodide (50 µg/ml; Sigma-Aldrich, Italy; prepared in PBS buffer) and RNase (HiMEDIA; 50 µg/ml) in a 10:1 ratio followed by slowly shaking in dark (37°C at room temperature). Untreated cells served as negative control.

Flow cytometric analysis was performed using Fluorescence assisted cell sorter (BD FACs Verse, USA) equipped with argon laser (15 mW, 488 nm, flow rate set at 100-1000 events per second upto a total of 10,000 events per sample). Forward scatter (FS), sideward scatter (SS) and relative fluorescence signals of individual cells were analyzed and plotted as logarithmic signals. Data analysis was done by BD FACSuite™ software.

3. Result and Discussion

3.1 Assessment of Photocatalytic Potentiality

UV-visible near infra-red absorption plots (Figures 1 a-d) against time function interval demonstrates higher degradation efficiency of Cu-NPs than CdS-NPs. Mineralization efficiency was calculated according to following equation[16].

Mineralization efficiency (%) = $[(A_0-A_t)/A_0]$, where A_0 = initial concentration of original dye, A_t = concentration of degraded dye after time t.

Residual concentration analyses reveal 78.0% and 72.0% MR dye removal (Figure 1 g) after 2h of visible light exposure by Cu- and CdS-NPs respectively. Increase of irradiation time shows disappearance of absorption peak of both the azo-dyes in a proportionate time function. Ratio of absorbance (A_0/A_t) (for both NPs) are plotted against time and can be seen to decrease with reaction

time for both MR and MG dyes (Figures 1 e,f). The logarithmic ratio between initial concentration of MR and MG dyes and the concentration after photolytic degradation [ln (A_0/A_t)] against corresponding irradiation time yield linear relationship for both nanocatalyst and seems to follow pseudo-first order kinetics.

For mineralization of MG, Cu-NPs demonstrate 1.5 folds upliftment in reaction potentiality than CdS-NPs (Figures 1 e, f). HPLC chromatograms of dye-NPs reaction system also exhibit enhancement in degradation potentiality of Cu-NPs than CdS-NPs which may be due to improved surface reactivity. Overlapping nature of valance and conduction band in metallic copper nanostructures possibly leads to rapid photo reactivation of the surface element. For CdS-NPs, persistent band gap between valance and conduction shell contributes to photo activation of the catalytic centre at higher time interval thereby reducing catalytic efficiency of the particle. However, in both NPs types, photo activation is associated with photon mediated excitation drive of ground state electron to conduction band. Such photo generated phenomenon is therefore responsible for the formation of electron-hole in valance band as well as excited electron localization in conduction band[17]. In the reaction system, electron-holes in the valance band oxidize water (H_2O) molecule leading to the formation of super active hydroxyl radicle ($OH^{\cdot}$)[18]. At conduction band reaction centre, a photoexcited electron are scav-

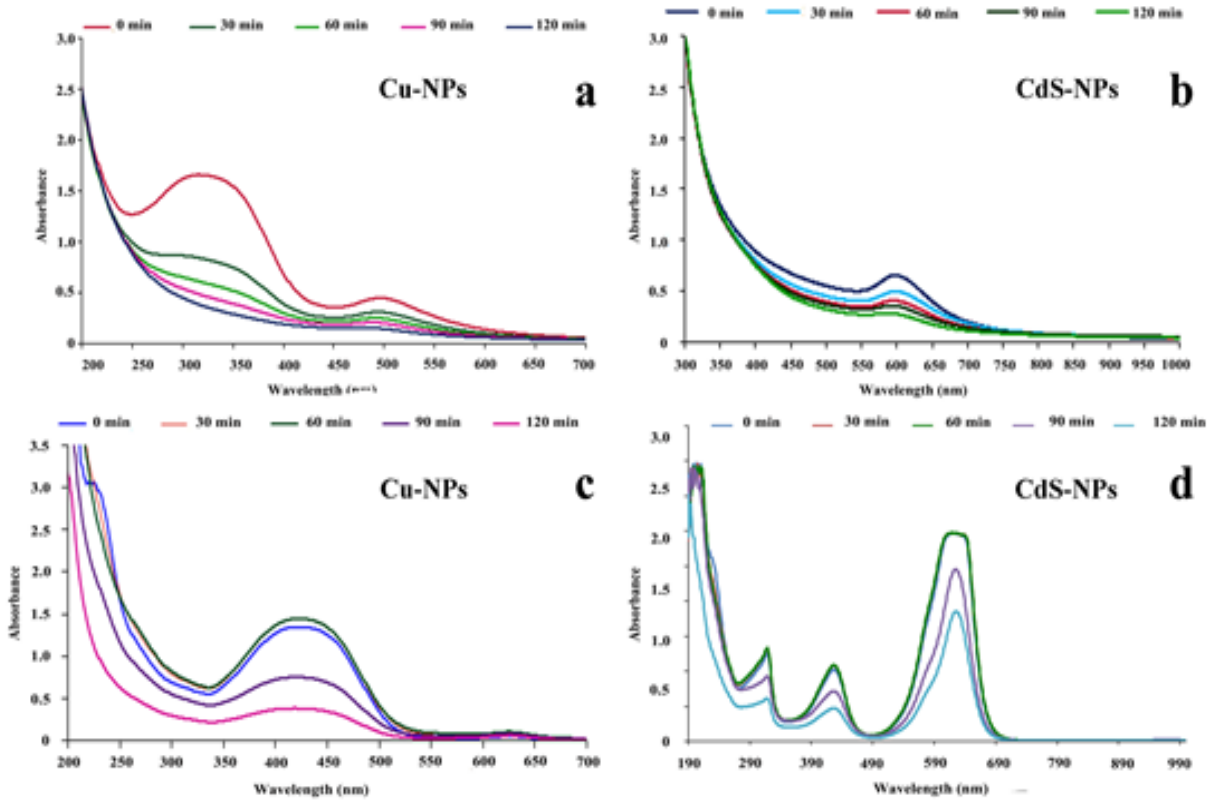

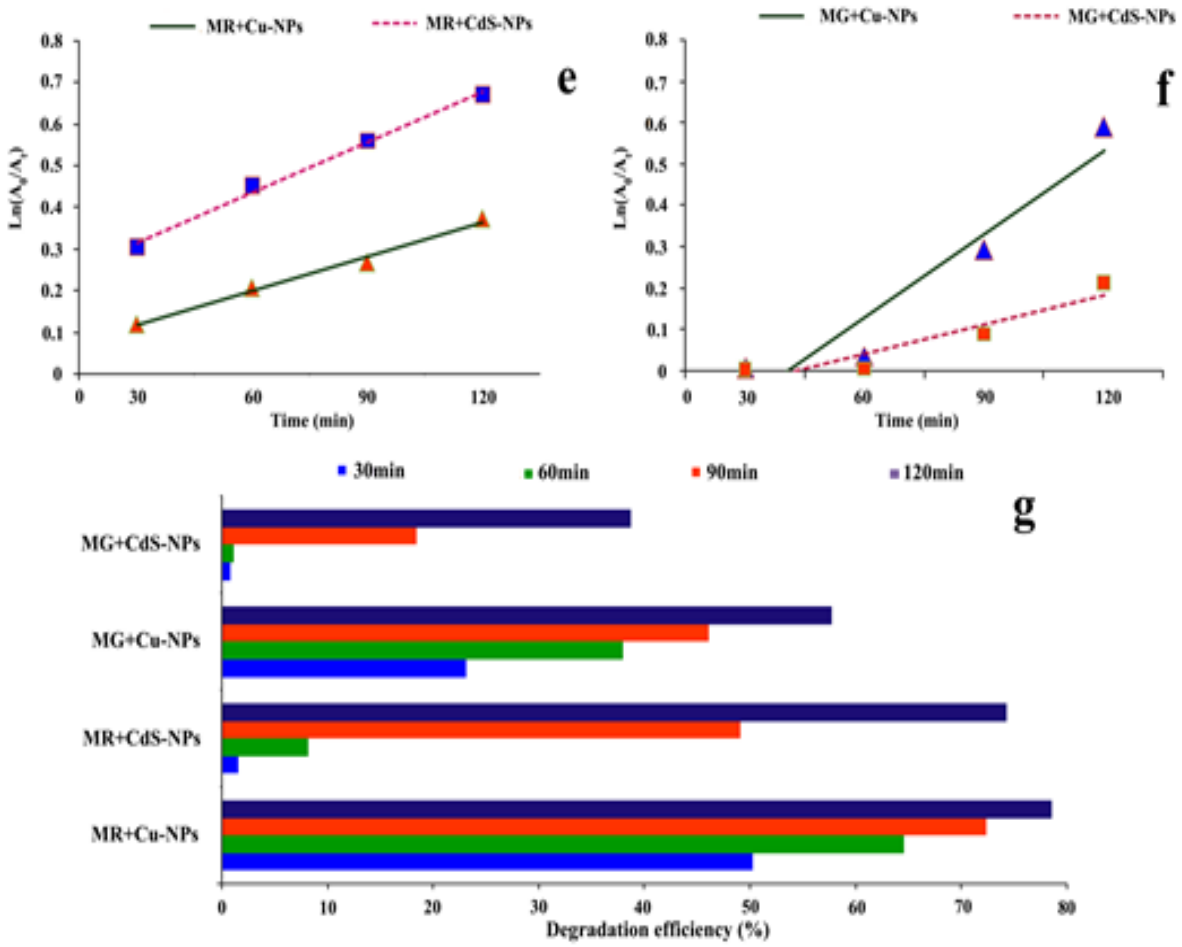

Figure 1. (A-d) UV visible spectra of photo catalytically degrading MR (a, c) and MG (b, d) at different time interval. Natural logarithmic plots (e-f) showing catalytic efficiency of different studied NPs. Bar histogram (g) showing dye mineralization at different NPs treating durations.

enged by the oxygen molecule persisting at the surface of nanomaterials and in turn produces super oxides (O_2^-). Both the hydroxyl and superoxide radicles prevailing at the nano surface act as organic azo-dye degrading reaction center. Hydroxyl and nucleophilic attack reaction by OH^- and O_2^- leads to subsequent mineralization of the dye compound[19,20].

3.2 Mechanism of Dye Degradation

Application of HPLC coupled with ESI-MS harvest positive insight about the mechanism of MR (Figures 2 a, c, e) and MG (Figures 2 b, d)dye degradation by NPs (Table 1). Intermediate compound identification (from online spectral library of National Institute

of Standard and Technology (www.nist.gov/pml/atomic-spectra-database) and analysis reveals two simultaneously occurring degradation pathways for both the azo-dyes (Figures 3-6).

Mineralization route for MR dye varies between the catalysts (Cu- and CdS-NPs) as evinced from intermediate compound identification. Cu-NPs mediated MR dye photolytic break down involves primary $OH^{\cdot}$ radicle driven attack reaction on the aminic side chain resulting demethylation and subsequent addition of hydrogen atom. Recurrent methyl group substitution reaction results in aromatic ring opening followed by complete dye mineralization. For CdS-NPs, primary degradation steps involve hydroxylation of aromatic benzene ring followed by another OH group addition in carboxyl radicle containing second aromatic ring. Reaction proceeds further by breaking central azo-bond (–N=N–) of the dye resulting in evolution of small molecular weight compounds.

For malachite green, resulting by-products analysis reveals two simultaneously occurring degradation routes by Cu-NPs. First route involves photolytic breakdown of (–N–CH_3–) bond of amino group yielding methyl group substituted (by hydrogen atom) by-products (m/z: 310, 318). Further, functional group substitution at the same nitrogen leads to the production of second by-products. Second route in Cu-NPs mediated MG mineralization path is nearly similar to the route prevailing in CdS-NPs. The pathway involves immediate removal of 3rd aromatic ring possibly through a hydrolysis mechanism. Reaction progresses further by two separate sub-routes either involving benzene ring opening in the truncated com-

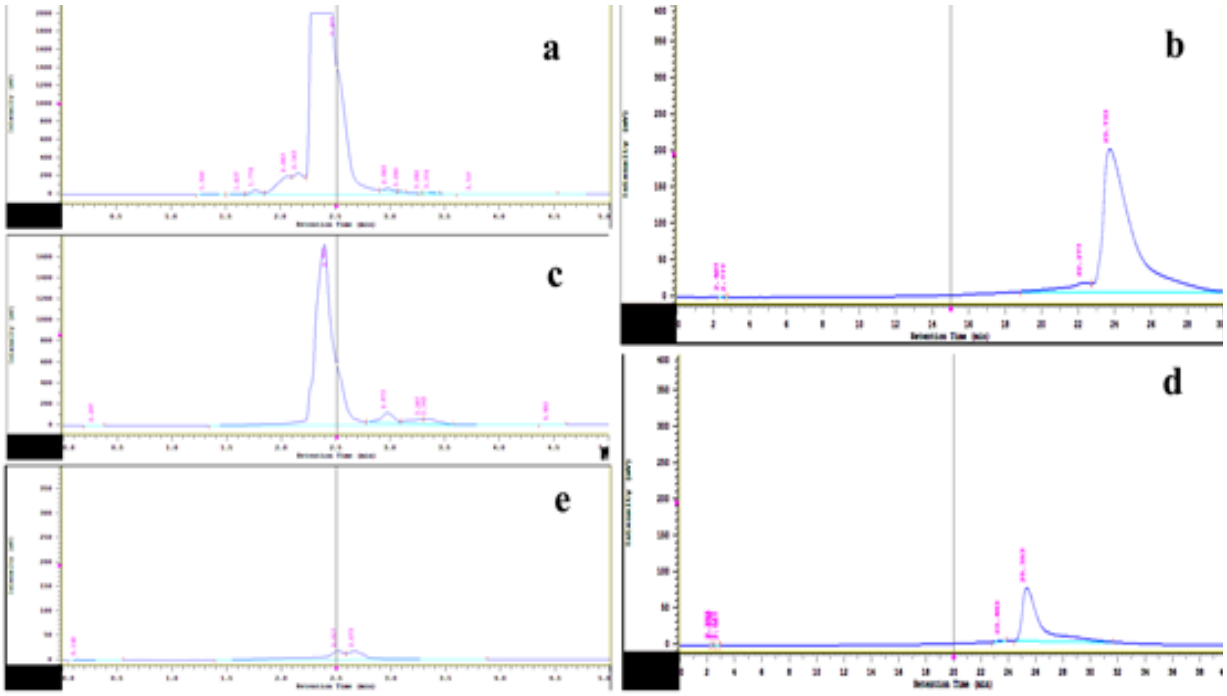

Figure 2. HPLC chromatograms showing MR (a, c, e) and MG (b, d) specific peak intensity at different photocatalytic interval.

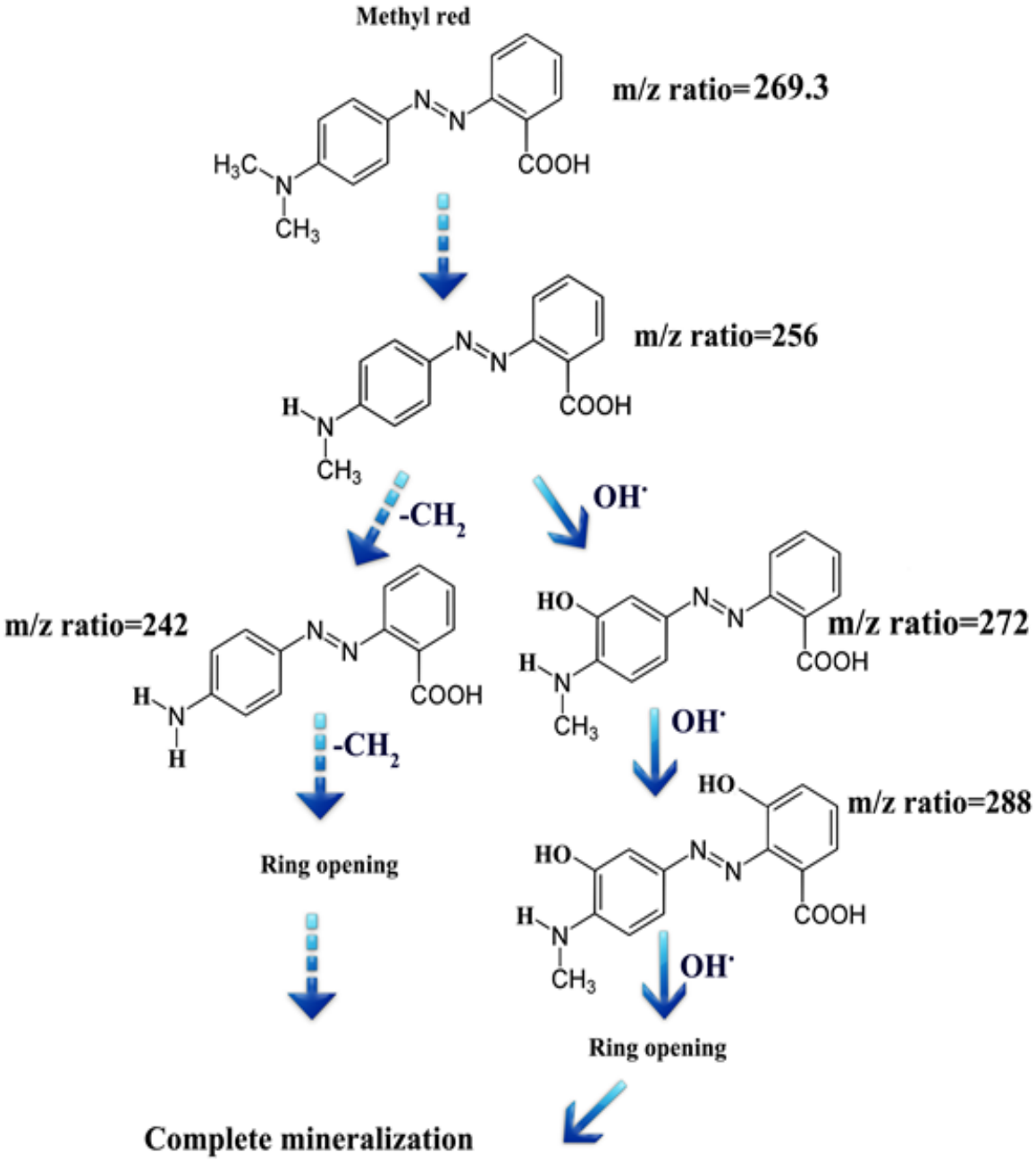

Figure 3. Schematic diagram showing MR degradation pathway under Cu-NPs mediated photo catalysis.

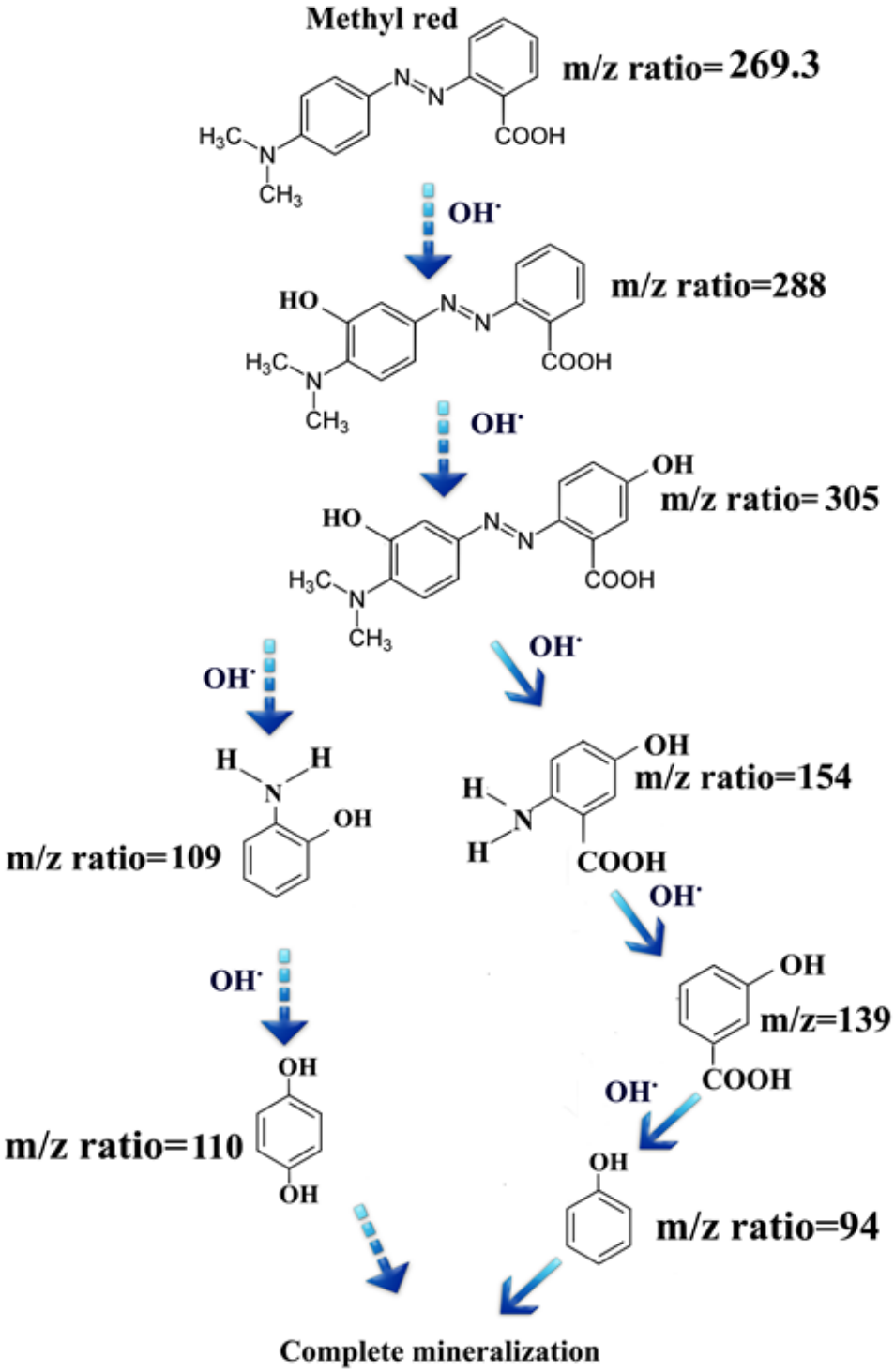

Figure 4. Diagrammatic representation depicting MR mineralization route following CdS-NPs driven photo catalysis.

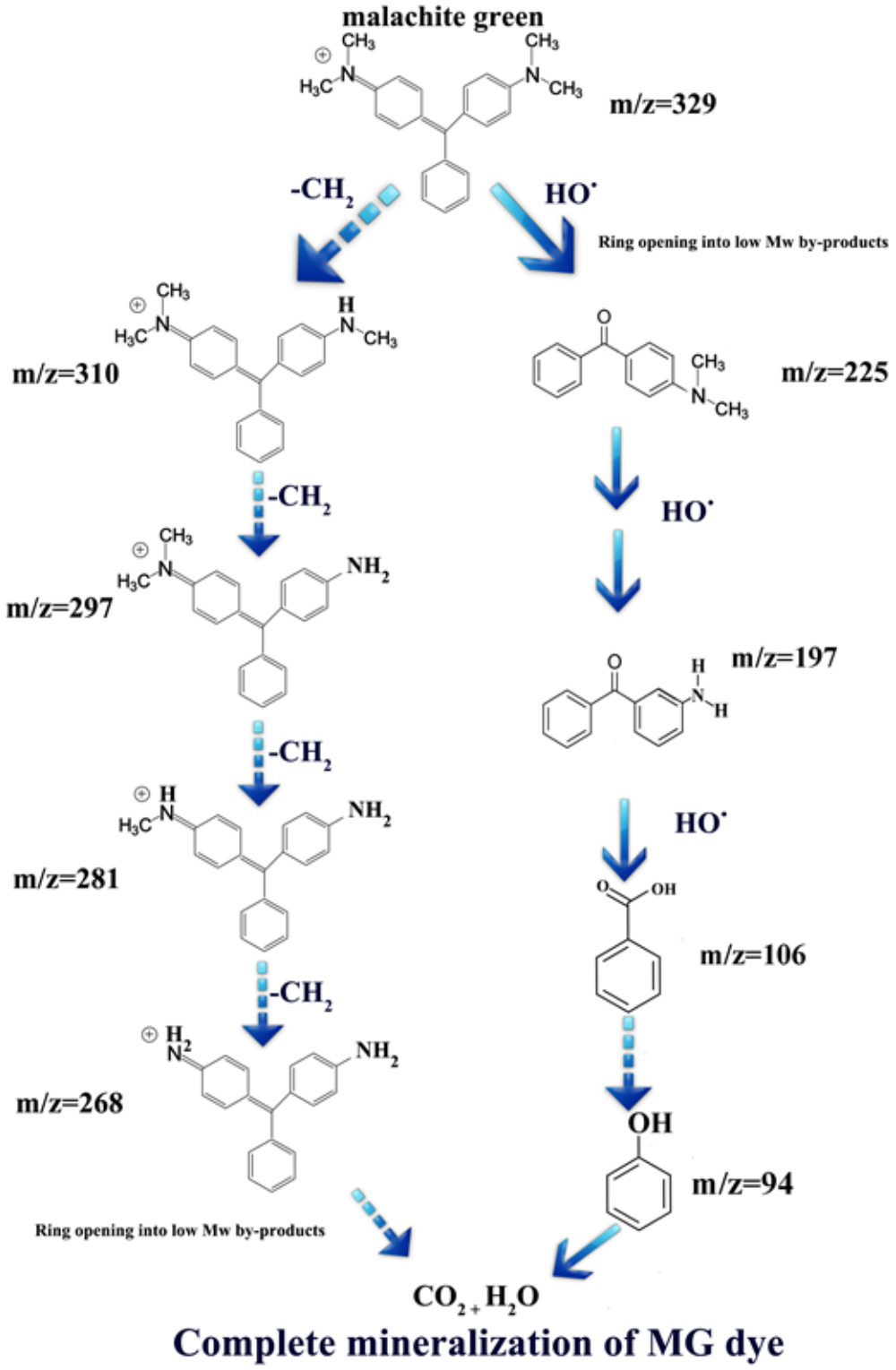

Figure 5. Scheme of photocatalytic degradation pathway of MG dye under Cu-NPs.

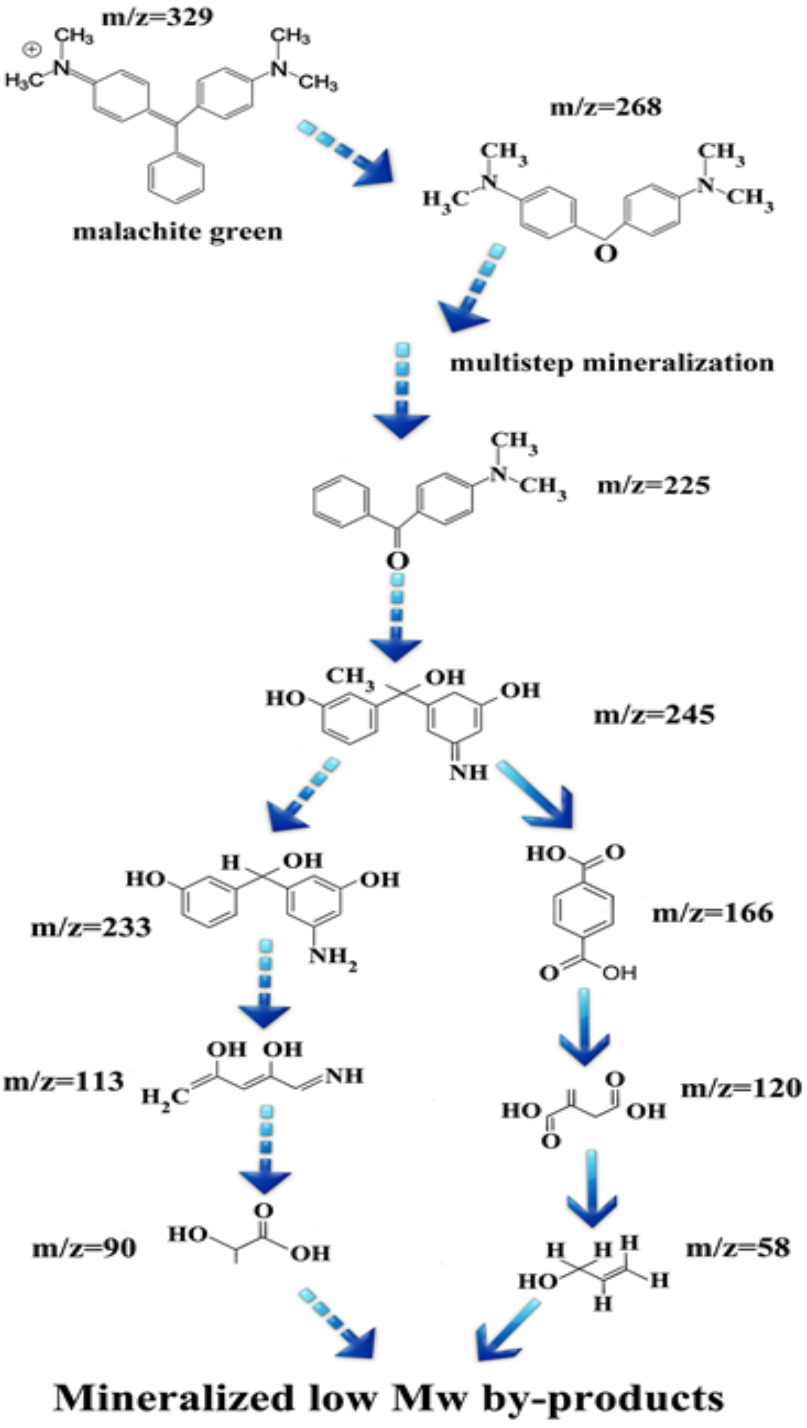

Figure 6. Proposed reaction pathway of CdS-NPS driven MG photolysis.

Table 1. ESI-QTOF-MS detection of by-products formed during dye degradation

Dye	Intermediate by-products (m/z)	Photo catalysis	
		Cu-NPs	CdS-NPs
Methyl red	305	-	+
	288	+	+
	269.3	+	+
	272	+	-
	256	+	-
	242	+	-
	154	-	+
	139	-	+
	110	-	+
	109	-	+
	94	-	+
Malachite green	329	+	+
	310	+	-
	297	+	-
	281	+	-
	268	+	+
	245	-	+
	233	-	+
	225	+	+
	197	+	-
	184	+	-
	166	-	+
	120	-	+
	113	-	+
	106	+	-
	94	+	-
	90	-	+
	58	-	+

pounds by hydroxylation or by ring separation through hydrolysis.

At the later stage, both reaction routes got interconnected and partially degenerated to form small molecular weight compounds [m/z: MG - 58, 90, 94; MR – 94, 110, 122, 138] before achieving complete mineralization. Difference in chemical nature, nanocrystal morphology, varied degree of electron affinity, dye adsorb potentiality, among others, are the possible contributing factors for diverse range of dye degradation pathways prevailing in different nanocatalytic systems (Cu-NPs and CdS-NPs).

3.3 Assessment of Antimicrobial Efficiency

3.3.1 Disc Diffusion Assay

From the zone of inhibition (Figures 7 a-j), it is evident that CdS-NPs possess strong antimicrobial potentiality against both *L. monocytogenes* isolates (causing listeriosis-disease relating to nervous system) and *S. typhimurium* (typhoid) for all the tested concentrations with maximum effectivity at 20 µg/ml (Figures 7 c, f, i). However, the studied inhibition zone is less than that assessed with ampicillin (Figures 7 a, d, g). *S. typhimurium* is found to

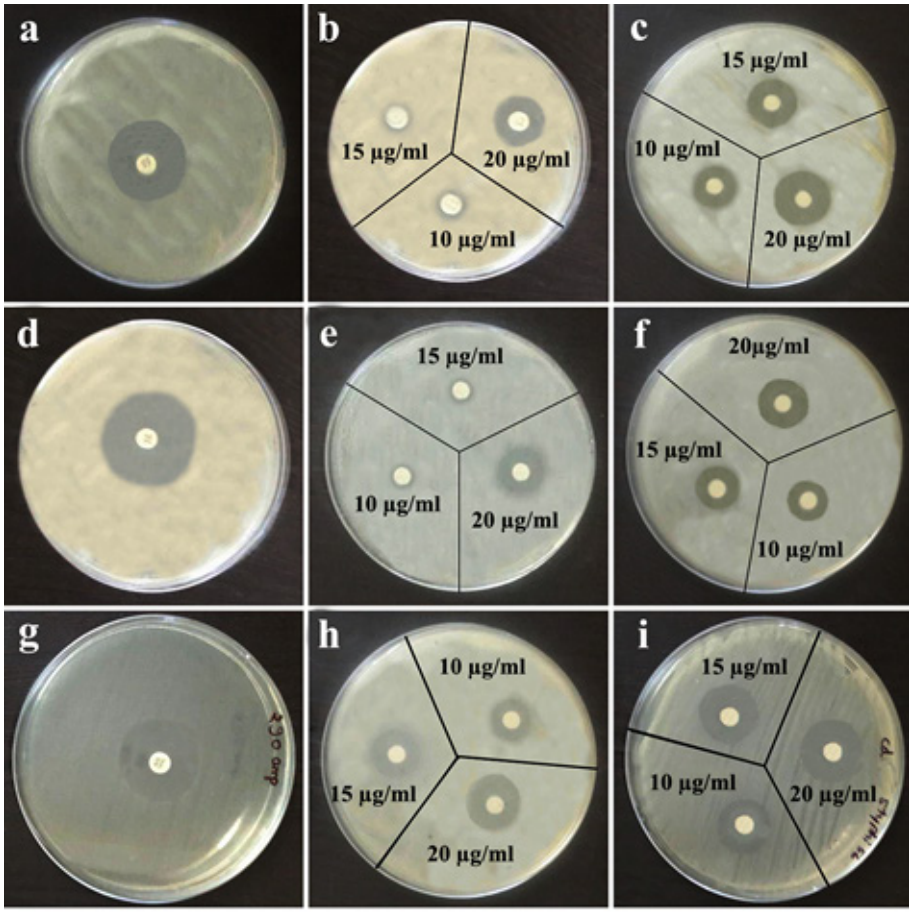

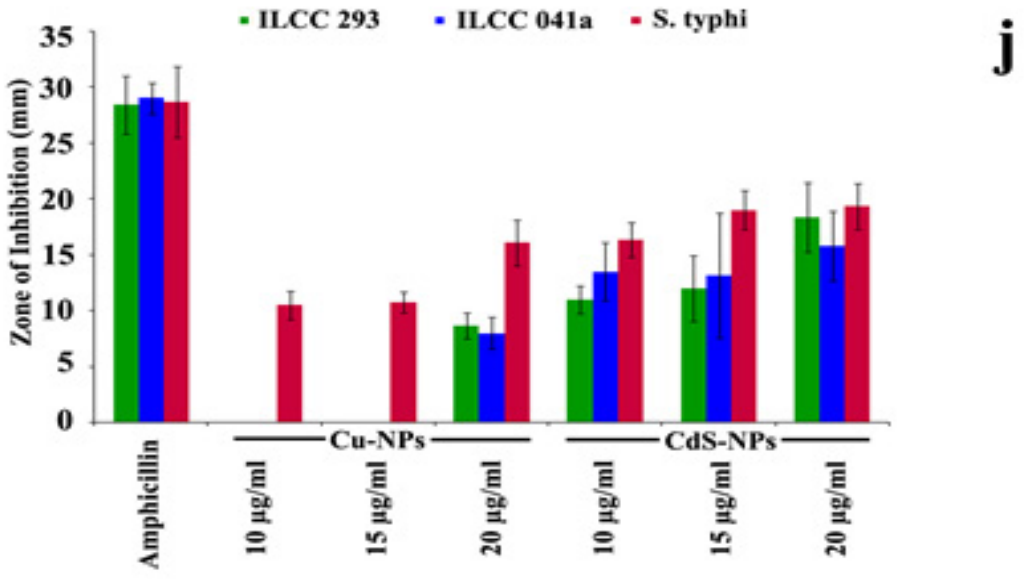

Figure 7. Bacterial plating showing zone of inhibitions in *L. monocytogenes* –ILCC 293 (a-ampicillin control, b-Cu-NPs, c-CdS-NPs), *L. monocytogenes* –ILCC 041a (d-ampicillin control, e-Cu-NPs, f-CdS-NPs) and *S. typhimurium* (g-ampicillin control, h-Cu-NPs, i-CdS-NPs). Bar histogram (j) representing zone of inhibitions in Cu- and CdS-NPs treated *L. monocytogenes* and *S. typhimurium* isolates.

be susceptible to Cu-NPs in all the tested concentrations ((Figure 7 h) but Cu-NPs show inhibition zone only at 20 µg/ml concentration for both *L. monocytogenes* isolates (Figures 7 b, e.) Results manifest that CdS-NPs can be used as an effective drug resource against listeriosis and typhoid. Cu-NPs can also be used for control of typhoid.

Cu-NPs are reported to show inhibition against *Staphylococcus aureus*, *Escherichia coli*, *Kleibsiella pneumonia*, *Pseudomonas aeroginosa*, *and Micrococcus luteus* among others[21]. The hydroxyl radical generated from metallic and ionic forms of Cu damages microbial DNA and proteins possibly resulting in both bacteriostatic and bactericidal effects[22]. CdS-NPs also exhibit antibacterial activity[23] due to its small size and high surface to volume ratio which increases Cd^{2+} ion release in microbial cell leading to cytotoxicity[24].

3.3.2 Flow Cytometry

FACs analysis of NPs treated bacterial suspensions exhibit changes in cell cycle progression (Figure 8). Untreated suspension show cell cycle consisting of normal G_1 and S/G_2 phases (Figure 8 a, d, g). while, treated cells show marked differences in cell cycle distribution (Figures 8 b, c, e, f, h, i). NPs treated bacterial suspensions represent apoptosis as evinced from sub-G_1 phase. Apoptotic cell death is higher in all CdS-NPs (Figures 8 c, f), i treated suspensions than Cu-NPs (Figures 8 b, e, h) Cell cycle arrest in all treated bacterial suspensions is found to occur

at G_1 phase (Figures 8 b, c, e, f, h), I In Cu-NPs, apoptotic cell death is near identical in all three bacterial suspensions; while, ILCC 293 demonstrates higher apoptotic cell death in CdS-NPs treatments compared to the other two bacterial isolates (Figure 8 j).

Earlier report shows that NPs attach bacterial cell membrane by electrostatic interaction followed by its internalization which changes microenvironment leading to ROS generation[25]. ROS produced may cause damage to bacterial cell membrane, DNA and mitochondria[11] cul-

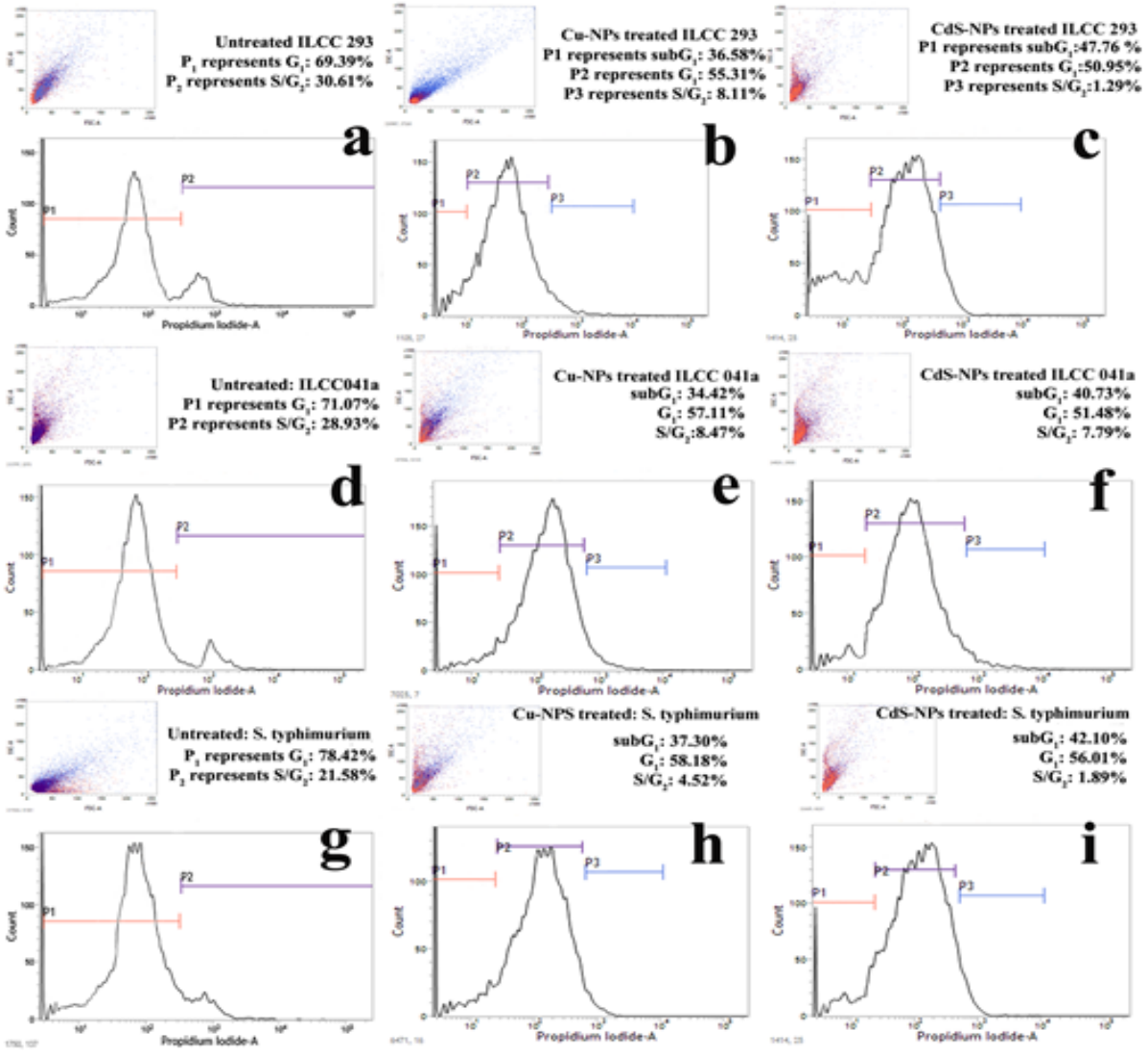

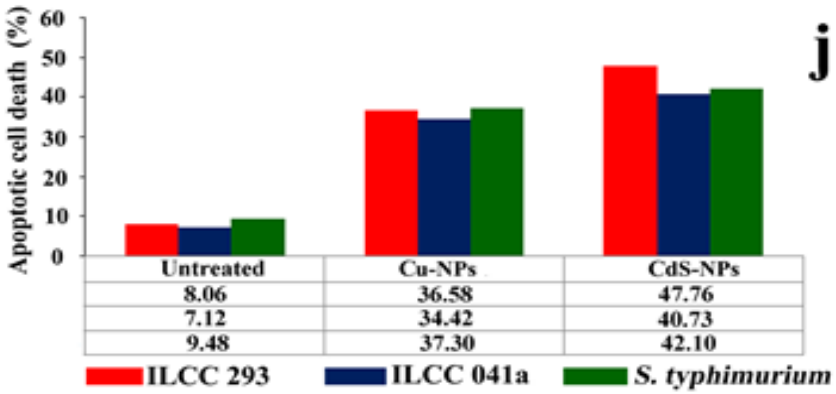

Figure 8. Flow cytometric analysis of all studied isolates under untreated (a, d, g), Cu- (b, e, h) and CdS-NPs (c, f, i) treatments. Bar histogram representing the apoptotic cell percentage in treatments (j).

minating in cell death. Nanomaterials possibly interact with microbial system resulting in malfunctioning of cell cycle check points which may in turn leads to blockage of cell cycle[26]. Apart from NPs imposed G_1 arrest, nanocrystal internalization beyond threshold limit also induce complete blockage of S phase leading to cell mortality and apoptosis[27].

4. Conclusions

Photolytic degradation pathways of the studied azo-dyes prevailing during photon-excited catalysis by both Cu- and CdS-NPs are novel and the identification of resultant intermediate compounds suggest prevalence of multiple interconnecting parallel routes rather than the previously reported bi-directional path of dye degradation. Furthermore, nanomaterials are found to possess antimicrobial potentiality in control of human pathogenic bacteria which may prove to be significant for drug designing and targeted delivery. Flow cytometric determination of antimicrobial activity of the studied CdS-NPs on different pathogenic serotypes of *Listeria monocytogenes* is novel and pioneer of its kind.

5. Acknowledgement

The Authors acknowledge the Joint Director, ICAR-NIBSM, Raipur for providing necessary permission for availing the facilities. The authors are also thankful to Bose Institue, Kolkata (FACs); Central Instrumentation Facilities, University of Kalyani (UPLC-ESI-QTOF-MS) and Department of Botany (HPLC and UV-vis), University of Kalyani for providing instrument facilities.

6. References

1. Roco MC. Broader societal issues of nanotechnology. Journal of Nanoparticle Research. 2003 Mar; 5(3-4):181–9.
2. Das D, Datta AK, Kumbhakar D, Ghosh B, Pramanik A, Gupta S. Conditional optimisation of wet chemical synthesis for pioneered ZnO nanostructures. Nanostructures and Nano-object. 2017 Jan; 9:26–30. Crossref.

3. Warrier P, Teja A. Effect of particle size on the thermal conductivity of nanofluids containing metallic nanoparticles. Nanoscale Research Letter. 2011 Mar; 6:247pp.
4. Cai J, Liu W, Li Z. One-pot self-assembly of Cu2O/RGO composite aerogel for aqueous photocatalysis. Applied Surface Science. 2015 Aug; 358:146-51.
5. Zou W, Zhang L, Liu L, Wang X, Sun J, Wu S, Deng Y, Tang C, Gao F, Dong L. Engineering the Cu2O-reduced graphene oxide interface to enhance photocatalytic degradation of organic pollutants under visible light. Applied Catalysis B: Environmental. 2016 Aug; 181:495-503.
6. Faisal M, Tariq MA, Muneer M. Photocatalysed degradation of two selected dyes in UV irradiated aqueous suspensions of titania. Dyes Pigments. 2007 Oct; 72(2):233–9. Crossref.
7. Bornick H, Schmidt TC. Organic pollutants in the water cycle. Properties, occurrence, analysis and environmental relevance of polar compounds. Wiley-VCH Verlag GmbH & Co. KGaA: Weinheim, Germany. 2006; 181–208.
8. Bhadwal AS, Tripathi RM, Gupta RK, Kumar N, Singh RP, Shrivastav A. Biogenic synthesis and photocatalytic activity of CdS nanoparticles. RSC Advances. 2014 Dec; 4(19):9484–90. Crossref.
9. Comparelli R, Fanizza E, Curri ML, Cozzoli D, Mascolo G, Agostiano A. UV-induced photocatalytic degradation of azo dyes by organic-capped ZnO nanocrystals immobilized onto substrates. Applied Catalysis B: Environmental. 2005 Mar; 60(1-2):1–11. Crossref.
10. Amini M, Ashrafi M. Photocatalytic degradation of some organic dyes under solar light irradiation using TiO2 and ZnO nanoparticles. Nanochemistry Research. 2016 Jul; 1(1):79–86.
11. Hajipour MJ, Fromm KM, Ashkarran AA, de Aberasturi DJ, de Larramendi IR, Rojo T, Serpooshan V, Parak WJ, Mahmoudi M. Antibacterial properties of nanoparticles. Trends in Biotechnology. 2012 Oct; 30(10):499–511. Crossref. PMid:22884769
12. Wang L, Hu C, Shao L. The antimicrobial activity of nanoparticles: present situation and prospects for the future. International Journal of Nanomedicine. 2017 Feb; 12:1227–49. Crossref. PMid:28243086 PMCid:PMC5317269
13. Kumbhakar DV, Datta AK, Mandal A, Das D, Gupta S, Ghosh B, Halder S, Dey S. Effectivity of copper and cadmium sulphide nanoparticles in mitotic and meiotic cells of Nigella sativa L. (black cumin) – can nanoparticles act as mutagenic agents? Journal of Experimental Nanoscience. 2016 Jan; 11(11):823–39. Crossref.
14. Chatterjee AK, Sarkar RK, Chattopadhyay AP, Aich P, Chakraborty R, Basu P. A simple robust method for synthesis of metallic copper nanoparticles of high antibacterial potency against E. coli. Nanotechnology. 2012 Feb; 23(8):085103. Crossref. PMid:22293320
15. Halder S, Mandal A, Das D, Datta AK, Chattopadhyay AP, Gupta S, Kumbhakar DV. Effective potentiality of synthesised CdS nanoparticles in inducing genetic variation on Macrotyloma uniflorum (Lam.) Verdc. BioNanoScience. 2015 Jul; 5(3):171-80.
16. Tantak NP, Chaudhari S. Degradation of azo dyes by sequential Fenton's oxidation and aerobic biological treatment. Journal of Hazardous Materials. 2006 Aug; 136(3):698–705. Crossref. PMid:16488538
17. Nakaruk A, Kavei G, Sorrell CC. Synthesis of mixed-phase titania films by low-temperature ultrasonic spray pyrolysis. Materials Letters. 2010 Mar; 64(12):1365–8. Crossref.
18. Curri ML, Comparelli R; Cozzoli PD, Mascolo G, Agostiano A. Colloidal oxide nanoparticles for the photocatalytic degradation of organic dyes. Materials Science and Engineering: C. 2003 Jan; 23:285–9. Crossref.
19. Pelaez M, Nolan NT, Pillai SC, Seery MK, Falaras P, Kontos AG, Dunlop PSM, Hamilton JWJ, Byrne JA, OSheaf K, Entezari MH, Dionysiou DD. A review on the visible light active titanium dioxide photocatalysts for environmental applications. Applied Catalysis B: Environmental. 2012 Aug; 125:331–49. Crossref.
20. Cardoso LC Savedra RML, Silva MM, Ferreira GR, Bianchi RF, Siqueira MF. Effect of Blue Light on the Electronic and Structural Properties of Bilirubin Isomers: Insights into the Photoisomerization and Photooxidation Processes. The Journal of Physical Chemistry A. 2015 Aug; 119(34):9037–42. PMid:26247544
21. Ramyadevi J, Jeyasubramanian K, Marikani A, Rajakumar G, Rahuman AA. Synthesis and antimicrobial activity of copper nanoparticles. Materials Letters. 2012 Mar; 71:114–6. Crossref.
22. Wang S, Lawson R, Ray PC, Yu H. Toxic effects of gold nanoparticles on Salmonella typhimurium bacteria. Toxicology and Industrial Health. 2011 Jul; 27(6):547–54. Crossref. PMid:21415096 PMCid:PMC3766946
23. Shivashankarappa A, Sanjay KR. Study on Biological Synthesis of Cadmium Sulfide Nanoparticles by Bacillus licheniformis and its Antimicrobial Properties against Food Borne Pathogens. Nanoscience and Nanotechnology Research. 2015 Jul; 3(1):6–15.

24. Hossain ST, Mukherjee SK. Toxicity of cadmium sulfide (CdS) nanoparticles against Escherichia coli and HeLa cells. Journal of Hazardous Materials. 2013 Sep; 260:1073–12. Crossref. PMid:23892173
25. Heinlaan M, Ivask A, Blinova I, Bubourguier H, Kahru A. Toxicity of nanosized and bulk ZnO, CuO and TiO2 to bacteria Vibrio fischeri and crustacean Daphnia magna and Thamnocephalus platyurus. Chemosphere. 2008 Apr; 71(7):1308–16. Crossref. PMid:18194809
26. Wei L, Tang J, Zhang Z, Chen Y, Zhou G, Xi T. Investigation of the cytotoxicity mechanism of silver nanoparticles in vitro. Biomedical Materials. 2010 Aug; 5(4):044103. Crossref. PMid:20683123
27. Park EJ, Yi J, Kim Y, Choi K, Park K. Silver nanoparticles induce cytotoxicity by a Trojan-horse type mechanism. Toxicology in Vitro. 2010 Apr; 24(3):872–8. Crossref. PMid:19969064